AGU ADVANCING EARTH AND SPACE SCIENCE

Geophysical Research Letters®

Key Points:
- We present the first magnetospheric multiscale observations of agyrotropic electron distributions in the foreshock transients
- Accompanied with the agytropic electron distributions, clear signatures of magnetic reconnection are absent
- The agytropic electron distributions are formed by the electron finite gyroradius effect at electron-scale boundaries

Correspondence to:
B. -B. Tang and X. -C. Guo,
bbtang@spaceweather.ac.cn;
xcguo@spaceweather.ac.cn

Agyrotropic Electron Distributions in the Terrestrial Foreshock Transients

C.-H. Gao[1,2] [ID], **B.-B. Tang[1]** [ID], **X.-C. Guo[1]** [ID], **W. Y. Li[1]** [ID], **Y. V. Khotyaintsev[3]** [ID], **D. B. Graham[3]** [ID], **D. L. Turner[4]** [ID], **Z. W. Yang[1]** [ID], and **C. Wang[1,2]** [ID]

[1]State Key Laboratory of Space Weather, National Space Science Center, Chinese Academy of Sciences, Beijing, China, [2]College of Earth and Planetary Sciences, University of Chinese Academy of Sciences, Beijing, China, [3]Swedish Institute of Space Physics, Uppsala, Sweden, [4]Space Sciences Department, The Aerospace Corporation, El Segundo, CA, USA

Abstract Agyrotropic electron distributions are frequently taken as an indicator of electron diffusion regions of magnetic reconnection. However, they have also been found at electron-scale boundaries of the non-reconnecting magnetopause and are generated by the electron finite gyroradius effect. Here, we present magnetospheric multiscale observations of agyrotropic electron distributions in the foreshock region. These distributions are generated by the electron finite gyroradius effect after magnetic curvature scattering at a thin electron-scale boundary. Meanwhile, the signatures of magnetic reconnection are absent at this boundary. The test-particle simulation is adopted to verify the generation of the agyrotropic electron distributions by assuming one-dimensional magnetic geometry. These observations suggest that agyrotropic electron distributions can be more widely formed at electron-scale boundaries in space plasma environment.

Plain Language Summary The agytropic electron distributions, which could be unstable to generate high frequency electrostatic waves, reveal valuable information of electron dynamics at electron scales. However, due to electron's small mass, the related observational study becomes only possible with the high-resolution magnetospheric multiscale data. In this study, we show that the agyrotropic electron distributions can be also formed in the foreshock transients such as inside an hot flow anomaly, suggesting that agyrotropic electron distributions are ubiquitous in space plasma.

1. Introduction

Agyrotropic electron distributions are formed when there are electron-scale boundaries in the magnetic field and/or plasma (Bessho et al., 2016; Gao et al., 2021; Lapenta et al., 2017; Shay et al., 2016; Wetherton et al., 2020). Recently, these agyrotropic distributions have been widely reported in observations (e.g., Burch et al., 2016; Graham et al., 2017; Khotyaintsev et al., 2016; Li et al., 2020, 2021; Tang et al., 2022; Torbert et al., 2018; Zhou et al., 2019) and particle-in-cell simulations (e.g., Bessho et al., 2016; Hesse et al., 2014; Ng et al., 2011; Shay et al., 2016). These agyrotropic electron distributions, along with other signatures (such as intense current density and enhanced energy dissipation), are taken as direct observation indicators of electron diffusion regions in magnetic reconnection (e.g., Fuselier et al., 2017; Lenouvel et al., 2021; Webster et al., 2018). Besides, these distributions are associated with density gradients reaching beyond the electron diffusion region (Egedal et al., 2016, 2018). Further, the agyrotropic electron distributions can be unstable to generate high frequency plasma waves (e.g., upper hybrid waves and electron Bernstein waves), which can thermalize electrons through wave-particle interactions (Burch et al., 2019; Dokgo et al., 2020; Graham et al., 2017; Li et al., 2020, 2021; Tang et al., 2019).

Although agyrotropic electron distributions have been revealed in the vicinity of electron diffusion regions, recent studies indicate that the occurrence of agyrotropic electron distributions are not necessarily related to the reconnection. They can be formed due to the electron finite gyroradius effect at electron-scale boundaries of the non-reconnecting magnetopause (Gao et al., 2021; Tang et al., 2019). The agyrotropic electron distributions can also be formed due to the direct acceleration of a sufficiently strong and local electric field, that is, its electric potential is comparable to or even larger than the electron thermal energy, and its width is shorter than the electron thermal gyroradius (Gao et al., 2021). These results suggest agyrotropic electron distributions can be frequently formed in space, but they have been reported at the magnetopause and in the magnetotail so far.

Whether agyrotropic electron distributions can be observed in the regions other than the magnetosphere remains unknown.

There are various kinds of kinetic structures in front of Earth's bow shock, such as hot flow anomalies (HFAs), foreshock cavities, foreshock bubbles, and short large amplitude magnetic structures (SLAMS). Many of these structures present transient features and are named foreshock transients (FTs). FTs usually include a core with the number density and magnetic field strength lower than the background solar wind values and compression edge(s) with the density and magnetic field strength higher than the solar wind values (Schwartz et al., 1985, 2000; Zhang & Zong, 2020). FTs play a significant role in the mass, momentum, and energy transport from the solar wind into the magnetosphere and impact the whole magnetosphere–ionosphere system (e.g., Eastwood et al., 2011; Zhang & Zong, 2020; Zhang et al., 2010). Recently, some more complex kinetic-scale processes in FTs have been reported, such as magnetic reconnection (Liu et al., 2020), magnetic holes (Huang et al., 2022; Liu et al., 2021) and magnetic flux ropes (Bai et al., 2020). In this study, we present the first magnetospheric multiscale (MMS) (Burch et al., 2016) observations of the agyrotropic electron distributions in an hot flow anomaly (HFA) and the SLAMS. These distributions are generated by a similar process at the non-reconnecting electron-scale boundary in Tang et al. (2019). This study provides further evidence that agyrotropic electron distributions are ubiquitous in space plasma.

2. MMS Observations

MMS consists of four identical satellites, providing high-quality plasma and fields measurements. In this study, we use particle data from the fast plasma investigation (FPI, Pollock et al., 2016), magnetic field data from the fluxgate magnetometer (FGM, Russell et al., 2016) and electric field data from the electric field double probes (EDP, Lindqvist et al., 2016; Ergun et al., 2016).

HFAs are transient phenomena with greatly heated plasmas and substantial flow deflections (Turner et al., 2018; Zhang & Zong, 2020). Here, we present MMS observations of an HFA on 10 December 2018 (Figure 1a). The four MMS spacecraft, located at [9.62, 17.58, 5.04] Earth radii (R_E) in geocentric solar ecliptic (GSE) coordinates, are in a tetrahedron formation with an average separation of ~14 km. MMS 1 encounters the downstream edge of the HFA around 04:41:00 UT (marked by the vertical black line in Figures 1b–1g). The spacecraft passes through the core of the HFA from about 04:41:08 UT to 04:41:40 UT (marked by vertical dash lines) and crosses the HFA shock (marked by the vertical blue line) at 04:41:49 UT. Typical characteristics of the HFA are observed, including the decrease of the magnetic field (~2 nT, Figure 1b) and the ion density (N_i < 1 cm^{-3}, Figure 1c), the deflection of the ion flow (V_z > 200 km s^{-1} and V_x < −200 km s^{-1}, Figure 1d), and the increase of the ion temperature (T_i > 1,000 eV, Figure 1e). Using the rotation of the interplanetary magnetic fields (IMF) before and after the HFA, we estimate the normal direction of the IMF tangential discontinuity that is responsible for the formation of this HFA to be n_{td} = [0.70, −0.01, 0.71] (GSE). The normal direction of the HFA shock is estimated by using the four-spacecraft timing method, leading to n_{sh} = [0.89, 0.44, −0.09]. In the red-shaded time interval, MMS observes a strong current sheet ($|J_y|$ > 100 nA m^{-2}, Figure 1f), which is the focus of this study.

A detailed plot of the red-shaded time interval is presented in a boundary-normal (LMN) coordinate system based on minimum variance analysis (MVA) of **B** between 04:41:10.50 UT and 04:41:11.00 UT, given by **L** = [0.99, 0.12, −0.10], **M** = [−0.13, 0.98, −0.10] and **N** = [0.09, 0.12, 0.99] (GSE, Figure 2). From the four-spacecraft timing method, the boundary velocity **V$_n$** is ~250 × [0.15, 0.24, 0.96] km s^{-1} (GSE), roughly aligned with **N** (the angle is about 8°). Thus, the thickness of the current sheet (between 04:41:10.76 UT and 04:41:10.88 UT) is about 30 km, which is comparable with the local electron thermal gyroradius (~18 km). Across this electron-scale current sheet, MMS observes a significant gradient of electron pitch-angle spectrum of energies between 50 and 130 eV with pitch angles around 90° (Figure 2h), which can be attributed to magnetic curvature scattering as the magnetic curvature radius R_c, defined by $\frac{R_c}{R_c^2} = (\frac{\mathbf{B}}{B} \cdot \nabla)\frac{\mathbf{B}}{B}$, is comparable to the local electron gyroradius ρ_e. Figure 2g shows the adiabatic parameter κ^2 defined by $\kappa^2 = R_c/\rho_e$ is below 10 or less, implying that the electron orbits become chaotic (Büchner & Zelenyi, 1989). Three electron distributions from 04:41:10.798 UT to 04:41:10.888 UT are presented in the planes perpendicular to the local magnetic fields, showing clear agyrotropic features of energies between 50 and 130 eV (Figures 2i–2k). We suggest they are formed by the finite gyroradius effect at the electron-scale boundary, where electron energy fluxes present significant gradient at pitch angles around 90° (Figure 2h), which is similar to that at the non-reconnecting magnetopause (Gao et al., 2021; Tang et al., 2019).
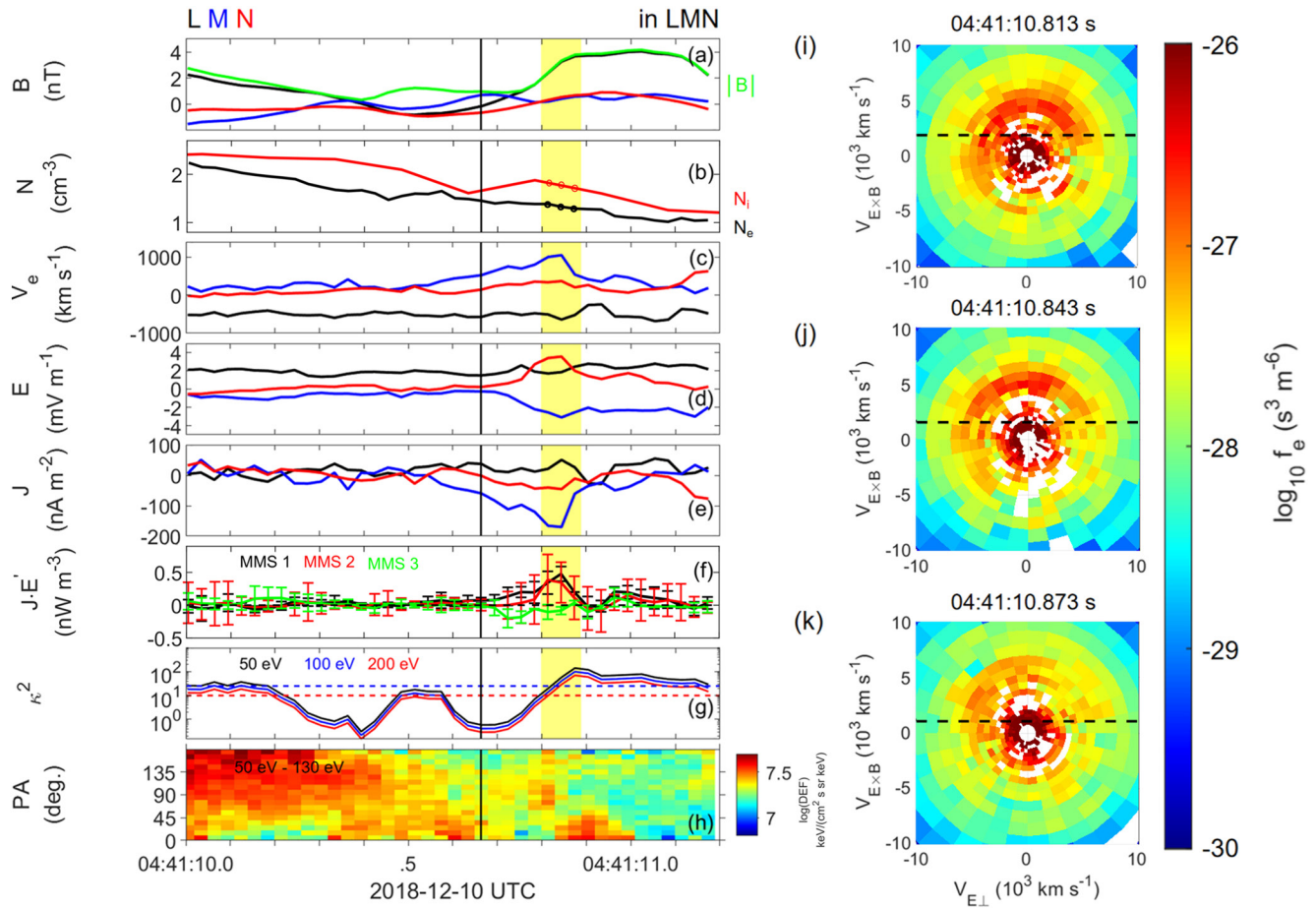
Figure 1. MMS1 observations of an hot flow anomaly (HFA) on 10 December 2018. (a) A schematic plot of the HFA structure and the magnetospheric multiscale crossing. (b) Magnetic field **B**. (c) Electron and ion number densities N. (d) Ion bulk velocity $\mathbf{V_i}$. (e) Ion parallel and perpendicular temperature $T_\parallel$ and $T_\perp$. (f) Current density **J** from the fast plasma investigation plasma moments. (g) Ion omni-directional differential energy flux. All vectors are presented in geocentric solar ecliptic coordinates. The vertical black line marks the downstream edge of the HFA and the vertical blue line marks the HFA shock. The two vertical dash lines mark the boundaries of the HFA core.

Another interesting question is whether these agyrotropic electron distributions are accompanied with magnetic reconnection. First, the electron outflow jet is reported as a character of magnetic reconnection in the transition region of the Earth's bow shock (Gingell et al., 2020; Wang et al., 2019). In this event, there is a peak of the electron velocity (>800 km s^{-1}) in the **M** direction, which is consistent with the magnetic B_L change. The V_{eL} is almost steady at ~-500 km s^{-1}, with a root mean square error δV_{eL} at ~80 km s^{-1} during the time interval in Figure 2c. Close to the B_L change, the relative change of the V_{eL} is about 30 km s^{-1}, which is less than δV_{eL} and the local Alfvén speed V_A (~50 km s^{-1}, based on B_L of 3–4 nT and N_e of 1.4 cm^{-3}). Thus, the outflow

Figure 2. Agyrotropic electron distribution functions in the hot flow anomaly core. (a) **B**. (b) Electron and ion number densities N. (c) Electron bulk velocity $\mathbf{V_e}$. (d) Electric field $\mathbf{E}$. (e) $\mathbf{J}$. (f) Energy conversion in electron-rest frames $\mathbf{J} \cdot \mathbf{E}'$ where $\mathbf{E}' = \mathbf{E} + \mathbf{V_e} \times \mathbf{B}$. (g) Electron adiabatic parameter defined by $\kappa^2 = R_c/\rho_e$, where the magnetic curvature radius R_c is calculated by using four-spacecraft magnetic field data, and ρ_e is the electron gyroradius. Here we show κ^2 of 50, 100 and 200 eV electrons. (h) Electron pitch-angle spectrum of energies between 50 and 130 eV. All vectors are in local LMN coordinates. (i–k) Electron distribution function slices in the $V_{E\perp}$–$V_{E\times B}$ planes at the three times highlighted by the yellow-shaded bar in panels (a–g) and by dots in panel (b). The black dashed lines in panels (i–k) mark $\mathbf{E} \times \mathbf{B}$ drift speed. The vertical black line indicates the selected time for the gyrotropic electron distributions in Figure 3b.

jet is not obvious here. Second, the nonideal energy conversion between the magnetic field and the particles, represented by $\mathbf{J} \cdot \mathbf{E}' = \mathbf{J} \cdot (\mathbf{E} + \mathbf{V_e} \times \mathbf{B})$, is enhanced in the previous reconnection events (Gingell et al., 2020; Wang et al., 2019; Wilder et al., 2018). In this event, $\mathbf{J} \cdot \mathbf{E}'$ from MMS 1–3 are almost negligible, if considering the uncertainties from the electric field (~3–8 mV m^{-1} from different MMS spacecraft) and the electron bulk velocity (~5–6 km s^{-1}, Figure 2f). Based on these arguments, we conclude that the observed electron agyrotropic distributions generated at the thin electron-scale boundary are not related to on-going magnetic reconnection.

3. Test Particle Analysis

We use the test particle method to reproduce the agyrotropic electron distributions in this event, and the detailed procedure is listed as follows. First, the magnetic field can be roughly taken as a one-dimensional structure based on the minimum directional derivative method (Shi et al., 2019). Second, we divide the magnetic field into three parts (04:41:10.00 UT–04:41:10.43 UT, 04:41:10.43 UT–04:41:10.81 UT and 04:41:10.81 UT–04:41:11.20 UT), which are colored in red, green and blue (Figures 3a and 3d). In the red and blue parts, the magnetic field is mostly along the **L** direction, and in the green part, the strength of the magnetic field is small (~1.5 nT). According to the boundary speed $\mathbf{V_n}$, the width of the each part along the **N** direction is about 100 km. The trajectory of a test particle with an initial energy of 105 eV and an initial pitch angle of 135° is also illustrated in Figure 3a. It is noted that we include the observed electric field in this test particle simulation. By comparing
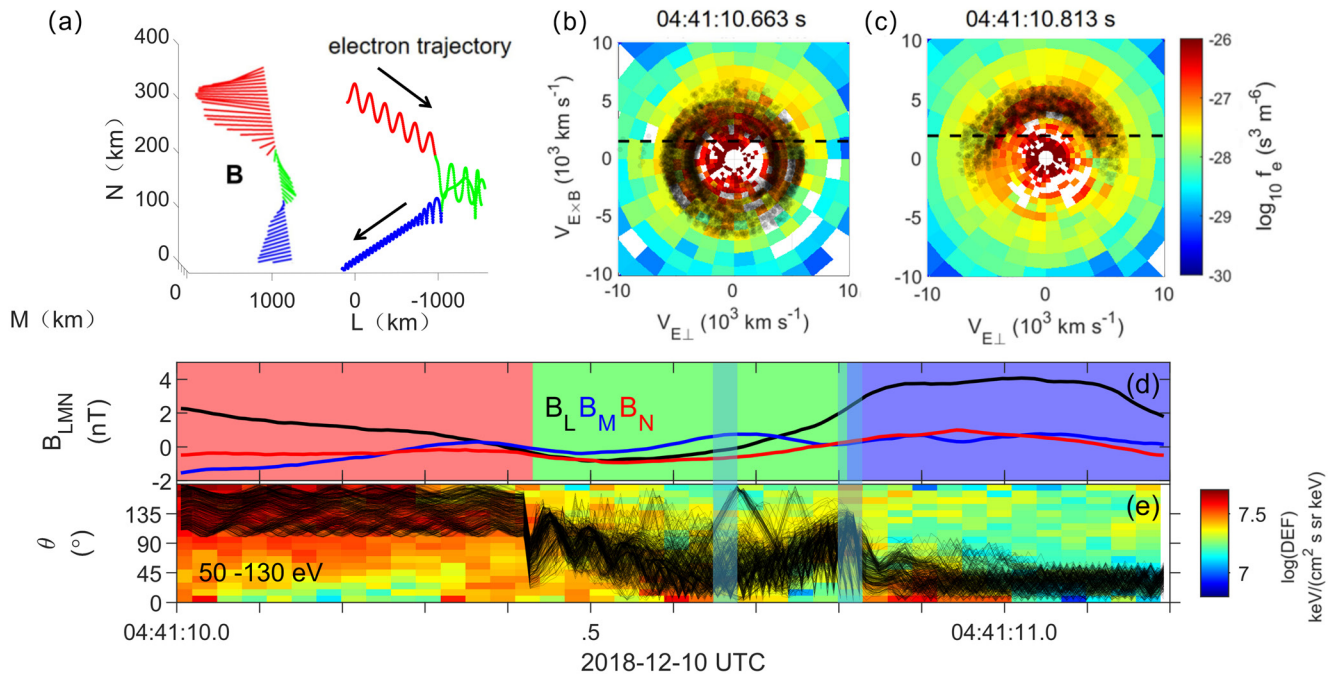
Figure 3. Test particle results of the agyrotropic electrons inside the hot flow anomaly. (a) Magnetic field geometry and an example of the test particle trajectories. (b, c) Observed electron distributions at the shaded time intervals in panels (d, e). The electrons with pitch angle between 70° and 110° in the test particle simulations are collected during the same time interval, and their trajectories in velocity space are overplotted in black. The black dashed lines in panels (b, c) mark $\mathbf{E} \times \mathbf{B}$ drift speed. (d) $\mathbf{B}$, which is divided into three parts according to the different electron behaviors. (e) Electron pitch angle spectrum, overplotted with pitch angles of test electrons.

the test particle results without an electric field, we find the difference is not obvious (the source code can be found in the Data Availability Statement). This can be attributed to the relatively weak electric field (~2 mV/m), which can only play a limited role (Gao et al., 2021). We find that this test particle travels from the anti-parallel direction in the red part to the parallel direction in the blue part, and this can be attributed to the weak magnetic field in the green part, in which the magnetic moment is no longer well conserved. Finally, we put 500 electrons with initial pitch angles in the range of 105°–180° and initial energies in the range of 50–130 eV in the red part and trace their trajectories. Electron pitch angles of all these 500 electrons are overplotted with the observed electron pitch angle spectrum (Figure 3e). The electrons are first along the anti-parallel direction in the red part, then pitch angle scattered in the green part, and finally along the magnetic field in the blue part. This result is consistent with the observations.

Meanwhile, we collect the test particles around 90° (70°–110°) pitch angles at the two selected time intervals (shaded in blue in Figures 3d–3e), and overplot their trajectories in velocity space with the observed electron distributions (Figures 3b–3c). At 04:41:10.663 UT (marked by vertical black line in Figures 2a–2g), the electrons are almost gyrotropic, while at 04:41:10.843 UT, the electron distribution becomes agyrotropic. The test particle results consist with observations, supporting the scenario that the agyrotropic electron distribution in the HFA core is generated at the electron-scale boundary in the absence of reconnection.

4. Discussion and Summary

In this study, we have shown MMS observations of agyrotropic electron distributions in an HFA. These agyrotropic distributions are generated by electron scattering at a thin electron-scale boundary, which has been reproduced by the test particle method. As this generation process is similar to that at the magnetopause, which is not necessarily related to reconnection (Tang et al., 2019), we infer that agyrotropic electron distributions can be widely formed in space plasma. Short large amplitude magnetic structures are large amplitude magnetic structures with durations of a few seconds (Zhang & Zong, 2020). Here, we present another MMS event of SLAMS (Figure 4). Some SLAMS (14:06:28 UT, 14:06:35 UT and 14:06:52 UT) are identified by clear variations of the magnetic field and ions (Figures 4a–4f). Again, we focus on the time interval shaded in yellow. A zoom-in plot is presented
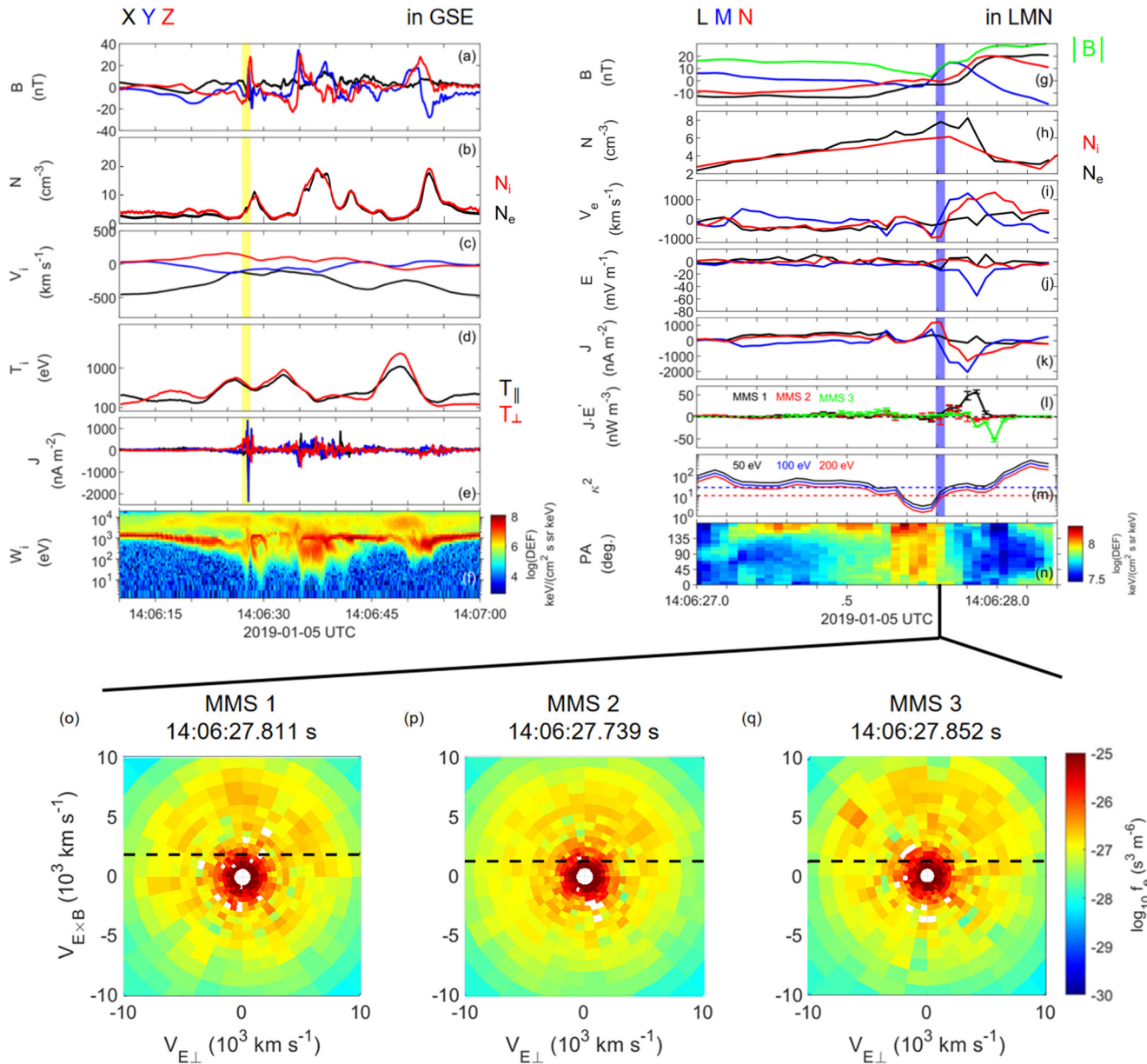
Figure 4. Agyrotropic electron distribution functions in short large amplitude magnetic structures. Top left: (a) **B**. (b) N. (c) $\mathbf{V_i}$. (d) $T_\parallel$ and $T_\perp$. (e) **J**. (f) Ion energy flux. Vectors in (a, c, and e) are in geocentric solar ecliptic coordinates. Top right panels (g–n) show the detailed observations in the interval denoted by the yellow bar in (a–e), using the same format as that in Figure 2, and the vectors are presented in LMN coordinates. (o–q) Electron distribution functions observed by Magnetospheric Multiscale 1–3 at the boundary denoted by the blue bar in (g–m), and black dashed lines mark the **E** × **B** drift speed.

in LMN coordinates based on the MVA method (**L** = [0.35, 0.29, 0.89], **M** = [0.51, 0.73, −0.44] and **N** = [−0.78, 0.61, 0.11], Figure 4g–4n). There are some fast magnetic rotations in this time interval, and at the time around 14:06:27.80 UT (shaded in blue), MMS 1 observes a significant gradient of electron energy flux around 90° pitch angles and clear agyrotropic electron distributions (Figures 4n and 4o). Similar agyrotropic electron distributions have also been found at MMS 2 and 3 (Figures 4p and 4q). As the estimated thickness of this magnetic boundary is about 12 km, comparable to the local electron thermal gyroradius (~5 km), we infer that these agyrotropic electron distributions are similarly generated by finite gyroradius effect. At this magnetic boundary, there is no obvious electron flows relative to the background (Figure 4i), and the energy conversion rate (**J** · **E**′) for MMS 1–3 (Figure 4l) are still negligible, although both of them change obviously later, corresponding with additional magnetic rotations. The reason why agyrotropic electron distributions are relatively rare to be observed in the

regions other than the magnetosphere can be attributed to fast plasma flows (such as in the foreshock regions), so that the electron-scale boundaries are more difficult to resolve.

In summary, we present two events of agyrotropic electron distributions observed in the foreshock region, that is, in an HFA and the SLAMS, respectively. They are generated by electron finite gyroradius effect at electron-scale boundaries, which can widely exist in FTs (e.g., turbulent fluctuations in the transient region). Further, in these two events, no obvious reconnection signal is observed, meaning agyrotropic electron distributions can be generated without reconnection. We reproduce the agyrotropic electron distributions at the electron-scale boundary in the 2018-12-10 HFA event from the test particle simulation, which confirms this generation process.

Although agyrotropic electron distributions can be generated without reconnection, we note that agyrotropic electron distributions in reconnection have some unique features. The reconnection electric field can accelerate electrons along the electron meandering orbits to form multiple agyrotropic electron crescents (Torbert et al., 2018), and in a single meandering orbit, the electron crescent can be tilted due to the acceleration by the reconnection electric field (Bessho et al., 2018). In addition, the reconnection guide field can facilitate agyrotropic electron distributions by distorting the electron meandering motion (Tang et al., 2022). All these results suggest that the formation of agyrotropic electron distributions in reconnection can be more complex than the simple scenario of the finite electron gyration at electron-scale boundaries without reconnection. Nevertheless, the agyrotropic electron distributions with/without reconnection can be unstable to drive high frequency plasma waves as previously reported, and the ubiquity of agyrotropic electron distributions in space suggests they can play a more important role to thermalize electrons by behaving as a possible source of free energy.

Data Availability Statement

The MMS data used in this work are available at the MMS Science Data Center (https://lasp.colorado.edu/mms/sdc/public/about/browse-wrapper). The MMS data analysis is performed with IRFU-Matlab package (https://github.com/irfu/irfu-matlab). The Matlab code for the test particles can be found at https://zenodo.org/record/7639193.

References

Bai, S.-C., Shi, Q., Liu, T. Z., Zhang, H., Yue, C., Sun, W.-J., et al. (2020). Ion-scale flux rope observed inside a hot flow anomaly. *Geophysical Research Letters*, *47*(5), e2019GL085933. https://doi.org/10.1029/2019GL085933

Bessho, N., Chen, L.-J., & Hesse, M. (2016). Electron distribution functions in the diffusion region of asymmetric magnetic reconnection. *Geophysical Research Letters*, *43*(5), 1828–1836. https://doi.org/10.1002/2016GL067886

Bessho, N., Chen, L.-J., Wang, S., & Hesse, M. (2018). Effect of the reconnection electric field on electron distribution functions in the diffusion region of magnetotail reconnection. *Geophysical Research Letters*, *45*(22), 12–142. https://doi.org/10.1029/2018gl081216

Büchner, J., & Zelenyi, L. M. (1989). Regular and chaotic charged particle motion in magnetotaillike field reversals: 1. Basic theory of trapped motion. *Journal of Geophysical Research*, *94*(A9), 11821–11842. https://doi.org/10.1029/JA094iA09p11821

Burch, J., Dokgo, K., Hwang, K., Torbert, R., Graham, D. B., Webster, J., et al. (2019). High-frequency wave generation in magnetotail reconnection: Linear dispersion analysis. *Geophysical Research Letters*, *46*(8), 4089–4097. https://doi.org/10.1029/2019gl082471

Burch, J., Torbert, R., Phan, T., Chen, L.-J., Moore, T., Ergun, R., et al. (2016). Electron-scale measurements of magnetic reconnection in space. *Science*, *352*(6290), aaf2939. https://doi.org/10.1126/science.aaf2939

Dokgo, K., Hwang, K.-J., Burch, J. L., Yoon, P. H., Graham, D. B., & Li, W. (2020). High-frequency waves driven by agyrotropic electrons near the electron diffusion region. *Geophysical Research Letters*, *47*(5), e2020GL087111. https://doi.org/10.1029/2020gl087111

Eastwood, J. P., Schwartz, S. J., Horbury, T. S., Carr, C. M., Glassmeier, K.-H., Richter, I., et al. (2011). Transient Pc3 wave activity generated by a hot flow anomaly: Cluster, Rosetta, and ground-based observations. *Journal of Geophysical Research*, *116*(A8), A08224. https://doi.org/10.1029/2011JA016467

Egedal, J., Le, A., Daughton, W., Wetherton, B., Cassak, P., Burch, J., et al. (2018). Spacecraft observations of oblique electron beams breaking the frozen-in law during asymmetric reconnection. *Physical Review Letters*, *120*(5), 055101. https://doi.org/10.1103/physrevlett.120.055101

Egedal, J., Le, A., Daughton, W., Wetherton, B., Cassak, P., Chen, L.-J., et al. (2016). Spacecraft observations and analytic theory of crescent-shaped electron distributions in asymmetric magnetic reconnection. *Physical Review Letters*, *117*(18), 185101. https://doi.org/10.1103/physrevlett.117.185101

Ergun, R., Tucker, S., Westfall, J., Goodrich, K., Malaspina, D., Summers, D., et al. (2016). The axial double probe and fields signal processing for the MMS misssion. *Space Science Reviews*, *199*(1–4), 167–188. https://doi.org/10.1007/s11214-014-0115-x

Fuselier, S., Vines, S., Burch, J., Petrinec, S., Trattner, K., Cassak, P., et al. (2017). Large-scale characteristics of reconnection diffusion regions and associated magnetopause crossings observed by MMS. *Journal of Geophysical Research: Space Physics*, *122*(5), 5466–5486. https://doi.org/10.1038/s41467-019-13920-w

Gao, C.-H., Tang, B.-B., Li, W. Y., Wang, C., Khotyaintsev, Y. V., Graham, D. B., et al. (2021). Effect of the electric field on the agyrotropic electron distributions. *Geophysical Research Letters*, *48*(5), e2020GL091437. https://doi.org/10.1029/2020GL091437

Gingell, I., Schwartz, S. J., Eastwood, J. P., Stawarz, J. E., Burch, J. L., Ergun, R. E., et al. (2020). Statistics of reconnecting current sheets in the transition region of Earth's bow shock. *Journal of Geophysical Research: Space Physics*, *125*(1), e2019JA027119. https://doi.org/10.1029/2019JA027119

Graham, D., Khotyaintsev, Y. V., Vaivads, A., Norgren, C., André, M., Webster, J., et al. (2017). Instability of agyrotropic electron beams near the electron diffusion region. *Physical Review Letters*, *119*(2), 025101. https://doi.org/10.1103/physrevlett.119.025101

Hesse, M., Aunai, N., Sibeck, D., & Birn, J. (2014). On the electron diffusion region in planar, asymmetric, systems. *Geophysical Research Letters*, *41*(24), 8673–8680. https://doi.org/10.1002/2014GL061586

Huang, S. Y., Wei, Y. Y., Zhao, J. S., Yuan, Z. G., Jiang, K., et al. (2022). Kinetic-size magnetic holes in the terrestrial foreshock region. *Geophysical Research Letters*, *49*(8), e2021GL093813. https://doi.org/10.1029/2021GL093813

Khotyaintsev, Y. V., Graham, D., Norgren, C., Eriksson, E., Li, W., Johlander, A., et al. (2016). Electron jet of asymmetric reconnection. *Geophysical Research Letters*, *43*(11), 5571–5580. https://doi.org/10.1002/2016GL069064

Lapenta, G., Berchem, J., Zhou, M., Walker, R. J., El-Alaoui, M., Goldstein, M. L., et al. (2017). On the origin of the crescent-shaped distributions observed by MMS at the magnetopause. *Journal of Geophysical Research: Space Physics*, *122*(2), 2024–2039. https://doi.org/10.1002/2016JA023290

Lenouvel, Q., Génot, V., Garnier, P., Toledo-Redondo, S., Lavraud, B., Aunai, N., et al. (2021). Identification of electron diffusion regions with a machine learning approach on MMS data at the Earth's magnetopause. *Earth and Space Science*, *8*(5), e2020EA001530. https://doi.org/10.1029/2020EA001530

Li, W.-Y., Graham, D., Khotyaintsev, Y. V., Vaivads, A., André, M., Min, e. a. K., et al. (2020). Electron Bernstein waves driven by electron crescents near the electron diffusion region. *Nature Communications*, *11*(1), 141. https://doi.org/10.1038/s41467-019-13920-w

Li, W.-Y., Khotyaintsev, Y. V., Tang, B.-B., Graham, D. B., Norgren, C., Vaivads, A., et al. (2021). Upper-hybrid waves driven by meandering electrons around magnetic reconnection X line. *Geophysical Research Letters*, *48*(16), e2021GL093164. https://doi.org/10.1029/2021GL093164

Lindqvist, P.-A., Olsson, G., Torbert, R., King, B., Granoff, M., Rau, D., et al. (2016). The spin-plane double probe electric field instrument for MMS. *Space Science Reviews*, *199*(1–4), 137–165. https://doi.org/10.1007/s11214-014-0116-9

Liu, T. Z., Lu, S., Turner, D. L., Gingell, I., Angelopoulos, V., Zhang, H., et al. (2020). Magnetospheric Multiscale (MMS) observations of magnetic reconnection in foreshock transients. *Journal of Geophysical Research: Space Physics*, *125*(4), e2020JA027822. https://doi.org/10.1029/2020JA027822

Liu, T. Z., Zhang, H., Turner, D. L., Goodrich, K. A., An, X., & Zhang, X. (2021). Kinetic-scale magnetic holes inside foreshock transients. *Journal of Geophysical Research: Space Physics*, *126*(10), e2021JA029748. https://doi.org/10.1029/2021JA029748

Ng, J., Egedal, J., Le, A., Daughton, W., & Chen, L.-J. (2011). Kinetic structure of the electron diffusion region in antiparallel magnetic reconnection. *Physical Review Letters*, *106*(6), 065002. https://doi.org/10.1103/PHYSREVLETT.106.065002

Pollock, C., Moore, T., Jacques, A., Burch, J., Gliese, U., Saito, Y., et al. (2016). Fast plasma investigation for magnetospheric multiscale. *Space Science Reviews*, *199*(1–4), 331–406.

Russell, C., Anderson, B., Baumjohann, W., Bromund, K., Dearborn, D., Fischer, D., et al. (2016). The magnetospheric multiscale magnetometers. *Space Science Reviews*, *199*(1–4), 189–256. https://doi.org/10.1007/s11214-014-0057-3

Schwartz, S. J., Chaloner, C. P., Christiansen, P. J., Coates, A. J., Hall, D. S., Johnstone, A. D., et al. (1985). An active current sheet in the solar wind. *Nature*, *318*(6043), 269–271. https://doi.org/10.1038/318269a0

Schwartz, S. J., Paschmann, G., Sckopke, N., Bauer, T. M., Dunlop, M., Fazakerley, A. N., & Thomsen, M. F. (2000). Conditions for the formation of hot flow anomalies at Earth's bow shock. *Journal of Geophysical Research*, *105*(A6), 12639–12650. https://doi.org/10.1029/1999JA000320

Shay, M. A., Phan, T. D., Haggerty, C. C., Fujimoto, M., Drake, J. F., Malakit, K., et al. (2016). Kinetic signatures of the region surrounding the X line in asymmetric (magnetopause) reconnection. *Geophysical Research Letters*, *43*(9), 4145–4154. https://doi.org/10.1002/2016GL069034

Shi, Q., Tian, A., Bai, S., Hasegawa, H., Degeling, A. W., Pu, Z. Y., et al. (2019). Dimensionality, coordinate system and reference frame for analysis of in-situ space plasma and field data. *Space Science Reviews*, *215*(4), 35. https://doi.org/10.1007/s11214-019-0601-2

Tang, B.-B., Li, W., Graham, D. B., Rager, A., Wang, C., Khotyaintsev, Y. V., et al. (2019). Crescent-shaped electron distributions at the nonreconnecting magnetopause: Magnetospheric multiscale observations. *Geophysical Research Letters*, *46*(6), 3024–3032. https://doi.org/10.1029/2019gl082231

Tang, B.-B., Li, W. Y., Khotyaintsev, Y. V., Graham, D. B., Gao, C. H., Chen, Z. Z., et al. (2022). Fine structures of the electron current sheet in magnetotail guide-field reconnection. *Geophysical Research Letters*, *49*(9), e2021GL097573. https://doi.org/10.1029/2021GL097573

Torbert, R., Burch, J., Phan, T., Hesse, M., Argall, M., Shuster, J., et al. (2018). Electron-scale dynamics of the diffusion region during symmetric magnetic reconnection in space. *Science*, *362*(6421), 1391–1395. https://doi.org/10.1126/science.aat2998

Turner, D., Wilson, L. B., Liu, T. Z., Cohen, I. J., Schwartz, S. J., Osmane, A., et al. (2018). Autogenous and efficient acceleration of energetic ions upstream of Earth's bow shock. *Physical Review Letters*, *561*(7722), 206–210. https://doi.org/10.1038/s41586-018-0472-9

Wang, S., Chen, L.-J., Bessho, N., Hesse, M., Wilson, L. B., III, Giles, B., et al. (2019). Observational evidence of magnetic reconnection in the terrestrial bow shock transition region. *Geophysical Research Letters*, *46*(2), 562–570. https://doi.org/10.1029/2018GL080944

Webster, J., Burch, J., Reiff, P., Daou, A., Genestreti, K., Graham, D. B., et al. (2018). Magnetospheric multiscale dayside reconnection electron diffusion region events. *Journal of Geophysical Research: Space Physics*, *123*(6), 4858–4878. https://doi.org/10.1029/2018ja025245

Wetherton, B. A., Egedal, J., Montag, P. K., Lê, A., & Daughton, W. S. (2020). A drift-kinetic method for obtaining gradients in plasma properties from single-point distribution function data. *Journal of Geophysical Research: Space Physics*, *125*(8), e2020JA027965. https://doi.org/10.1029/2020JA027965

Wilder, F. D., Ergun, R. E., Burch, J. L., Ahmadi, N., Eriksson, S., Phan, T. D., et al. (2018). The role of the parallel electric field in electron-scale dissipation at reconnecting currents in the magnetosheath. *Journal of Geophysical Research: Space Physics*, *123*(8), 6533–6547. https://doi.org/10.1029/2018JA025529

Zhang, H., Sibeck, D. G., Zong, Q.-G., Gary, S. P., McFadden, J. P., Larson, D., et al. (2010). Time history of events and macroscale interactions during substorms observations of a series of hot flow anomaly events. *Journal of Geophysical Research*, *115*(A12), A12235. https://doi.org/10.1029/2009JA015180

Zhang, H., & Zong, Q. (2020). Transient phenomena at the magnetopause and bow shock and their ground signatures. In *Dayside magnetosphere interactions* (pp. 11–37). American Geophysical Union (AGU). https://doi.org/10.1002/9781119509592.ch2

Zhou, M., Deng, X., Zhong, Z., Pang, Y., Tang, R., El-Alaoui, M., et al. (2019). Observations of an electron diffusion region in symmetric reconnection with weak guide field. *The Astrophysical Journal*, *870*(1), 34. https://doi.org/10.3847/1538-4357/aaf16f